Fuel Processing Technology 238 (2022) 107492

Contents lists available at ScienceDirect

Fuel Processing Technology

journal homepage: www.elsevier.com/locate/fuproc

Biofuel characteristics of chars produced from rapeseed, whitewood, and seaweed via thermal conversion technologies – Impacts of feedstocks and process conditions

Fatih Güleç [a,*], Abby Samson [b], Orla Williams [a], Emily T. Kostas [c], Edward Lester [a]

[a] Advanced Materials Research Group, Faculty of Engineering, University of Nottingham, Nottingham NG7 2RD, UK
[b] Department of Mechanical Engineering, University of Sheffield, Sheffield S3 7RD, UK
[c] Advanced Centre of Biochemical Engineering, Bernard Katz Building, University College London, Gower Street, London WC1H 6BT, UK

ARTICLE INFO

Keywords:
Char formation
Hydrothermal treatment
Pyrolysis
Torrefaction
Energy application

ABSTRACT

Understanding the suitability of different conversion technologies for different types of biomass feedstocks is crucial in delivering the full valorisation of different types of biomass feedstocks. Optimal valorisation pathways can be identified by investigating the formation of products and the most efficient application technologies of these products. This is therefore novel research reporting an extensive comparative study on the biomass processing pathways (hydrothermal conversion, pyrolysis, and torrefaction) for three distinct biomass feedstocks (Rapeseed residue, Whitewood, Seaweed–*Laminaria Digitata*) to optimise char formation under a wide range of processing conditions and their biofuel characteristics in the bioenergy applications. The results demonstrates that Whitewood gradually decomposes during all three conversion processes to produce chars (hydrochars/biochars) that have a lower O/C-H/C ratio as process temperature increases. The char formation from Whitewood follows the dehydration process in the Van Krevelen diagram. Char formation from Rapeseed residue and *L. digitata* via pyrolysis also follows a similar dehydration and demethanation pathway at higher temperatures (550 °C for Rapeseed residue and 400 °C for L. *digitata*). However, char formation from Rapeseed residue and L. *digitata* via hydrothermal conversion predominantly follows the decarboxylation pathway producing structures with a higher H/C ratio and lower O/C ratio. The intrinsic reactivity analysis of these chars showed that the temperature of initial weight loss and the onset of ignition for the raw biomass sample was shifted to a higher temperature for the chars produced by hydrothermal conversion or pyrolysis, regardless of biomass feedstocks. The chars produced from Whitewood (with hydrothermal conversion, pyrolysis and torrefaction) and Rapeseed residue (with pyrolysis) have a potential application in bioenergy production due to the significant enhancement of char products. However, the chars produced from L. *digitata* appear less promising for bioenergy applications due to relatively low energy yield, carbon recovery, inferior char structures and a high inherent ash content.

1. Introduction

Biomass can be an inexpensive, clean, and environmentally friendly energy source. It is mainly composed of three major components – hemicellulose, cellulose, and lignin [1–4]. With the potential to achieve net negative emissions from bioenergy and biofuels, biomass is a promising energy resource [5] that will continue to play an undeniable role in the 'net zero' energy transition [6,7]. In 2019, 19.7% of the EU's energy consumption was supplied by renewable energy sources [8], 60% of which came from bioenergy [9]. The European bioeconomy is now worth over €621 billion in added value benefits, representing 4.2% of EU GDP and employing 18 million people [10]. The demand for bioenergy in the EU is expected to increase to 32% by 2030 due to energy and climate change strategies [5,9].

Biofuels (solid, liquid, and gas) are produced through the thermal conversion of biomass feedstocks by utilising technologies such as hydrothermal conversion (carbonisation for hydrochar, liquefaction for value-added chemicals, and gasification for syngas) [11–13], pyrolysis (slow, fast, and flash for biochar, gas and oils) [14–16], and gasification (for syngas) [17,18]. Biomass feedstocks must be utilised sustainably and efficiently to prevent deforestation and other detrimental effects on ecosystems such as loss of biodiversity/habitats [9]. For successful

* Corresponding author.
E-mail addresses: Fatih.Gulec1@nottingham.ac.uk, Gulec.Fatih@outlook.com (F. Güleç).

https://doi.org/10.1016/j.fuproc.2022.107492
Received 6 June 2022; Received in revised form 1 August 2022; Accepted 2 September 2022
Available online 15 September 2022

commercialisation of bioenergy and/or bioproducts, consideration of numerous parameters is required, including biomass sourcing, differences in physical, chemical, and biological structures, cost-competitive bioproducts, effective biomass refinery technologies, and a stable supply chain [19–23]. Understanding the suitability of different conversion technologies for different types of biomass feedstocks is crucial in delivering the full valorisation of different types of biomass feedstocks. Optimal valorisation pathways can be identified by investigating the formation of products such as solids (hydrochar/biochar), liquids (bio-oil and biochemicals), and gases (potentially syngas) and the most efficient application technologies of these products.

The European Biochar Foundation defines biochars/hydrochars as "a heterogeneous substance rich in aromatic carbon and minerals" [24]. Biochars/hydrochars are stable, homogeneous solid fuels showing high energy densities and calorific values compared to the original biomass source [25,26]. Biochars/hydrochars are mainly produced by thermal conversion technologies leading to changes in chemical compositions of biomass [24,27]. Slow pyrolysis is one of the thermal conversion processes to produce "biochar" by utilising relatively low temperatures (ca. 400 °C), slow heating rates (2–7 °C/min), and long residence times (hours or days) under oxygen-free environments [16,21]. Hydrothermal carbonisation (HTC) is another low-temperature process used to produce "hydrochars" at subcritical conditions (180–250 °C,15–40 bar) [28,29]. In addition to these two technologies, biomass feedstocks can also be converted into medium grade biochars (also called torrefied biomass) via Torrefaction, which is a mild pyrolysis process conducted at 200–300 °C under low-oxygen or inert atmospheres [25,30,31]. The type of biomass feedstock and process conditions like temperature, pressure, residence time, and heat transfer rate have a major effect on the physicochemical properties of the produced biochar/hydrochar [24] pore structure, surface area, carbon content and surface functional groups [32,33]. The physicochemical properties of biochar/hydrochar play a crucial role in defining the application of these chars in the most efficient technology. Biochars/hydrochars could be used for agricultural soil enhancement and have been shown to improve the nutrient retention capacity of soils [34,35]. Additionally, chars can be used to immobilise contaminants (including heavy metals, dyes, and pharmaceuticals) from soil and wastewater [36–38]. Biochars/hydrochars can also be used in renewable energy production via combustion [9,31,39].

As biochars/hydrochars show very different physicochemical properties based on the preparation technology and conditions used, characterisation of these chars aids in identifying the most suitable production method for the desired application ensuring maximum valorisation of the biomass and chars [11]. To understand the potential of the biochar/hydrochar in energy applications, it is important to understand their chemical composition (C, H, O, N, and S) [11,40,41], proximate analysis (volatiles, fixed carbon, and ash content) [40,41], heating values, structural composition (hemicellulose, cellulose and lignin) [42,43], combustion characteristics (kinetics and intrinsic reactivity) [6,44,45], and the ratios of H/C and O/C [28,46]. The intrinsic reactivity of biochar can provide relatively useful information such as initial decomposition temperature, ignition temperatures, burnout temperature, maximum weight loss rate, average weight loss rates, combustion stability index and the comprehensive combustion index [7,47–49]. Van Krevelen diagram is a graphical method to characterise the source and maturity of organic matter by plotting atomic ratios of H/C versus O/C [50]. The position (state) of chars on this diagram can also provide information about the char structure and the impact of process conditions on char formation. Furthermore, it can potentially identify the char formation reaction path i.e. demethanation, dehydration, and/or decarboxylation (some examples of Van Krevelen Diagram and reaction paths are presented in Fig. Appendix A. in supplementary information) [46,51].

Although a wide range of biofuels characteristics has been presented for single type of biomass and biochars, there is a limited understanding on comprehensively investigation of biochars/hydrochars produced by distinct biomass feedstocks via different thermal conversion technologies in bioenergy application. This is the first comparative study on how the optimal holistic biomass processing pathways and process interdependencies are influenced by feedstocks for the optimisation of char formation and the subsequent bioenergy application of these chars. The suitability of three distinct biomass feedstocks (Whitewood, Rapeseed, and L. *digitata*) was investigated for char (hydrochar/biochar) formation in three specific thermal conversion technologies; torrefaction, pyrolysis, and hydrothermal conversion (subcritical conditions; hydrolysis, carbonisation, and liquefaction) under a wide range of processing conditions. This paper presents detailed bio-fuel characteristics of the chars (biochars/hydrochars) based on the carbon recovery, energy densification, and energy yield of chars. Char structures were identified by plotting the atomic ratio of H/C-O/C on the Van Krevelen diagram. The effects of the thermal conversion processes and conditions on char combustion behaviour were also investigated via intrinsic reactivity analysis.

2. Material and methods

2.1. Feedstocks and char characterisation

The three feedstocks used in this study, Rapeseed residue (RS, source of agricultural waste, supplied by the Bioscience Department of the University of Nottingham), Whitewood (WW, made from sawdust residues from Northern Ireland, supplied by Brites), and *Laminaria Digitata* (LD, UK sourced brown seaweed), were selected as they are all domestically produced in the UK [2,52,53]. The biomass feedstocks (RS, WW, LD) were ground into a powder and sieved into different particle sizes (106–212 μm, 212–300 μm, 300–425 μm, 425–600 μm) in a sieve shaker for 15 min according to EN ISO 17827-2:2016 [54,55]. Proximate analysis of the raw biomass and prepared chars was performed in a TA-Q500 using the procedure modified from the previous studies [2,56,57]. Furthermore, the elemental compositions (carbon (C), hydrogen (H), nitrogen (N)) of the biomass feedstocks were determined using a LECO CHN 628; oxygen (O) content was calculated by difference. Further details of proximate and ultimate analyses conditions have been presented in previous studies [58]. Among eleven different Higher Heating Value (HHV) correlations (presented in Table A1 supplementary information), the HHV correlation for each type of biomass feedstock was identified with the lowest standard deviations between the experimental and predicted HHV [59–61], as presented in Eqs. (1)–(3).

$$HHV = 0.2949C + 0.8250H \quad for\ Rapeseed \tag{1}$$

$$HHV = -3.440 + 0.517(C+N) - 0.433(H+N) \quad for\ Whitewood \tag{2}$$

$$HHV = 0.4373C - 1.6701 \quad for\ L.Digitata \tag{3}$$

where, HHV is higher heating value (kJ/g), C is the carbon content of biomass (wt%), H is the hydrogen content of biomass (wt%), N is the nitrogen content of biomass (wt%).

The trace metals and major elements in biomass were measured externally by Alfred H Knight company using the standard methods: ISO BS EN 16968:2015 [62] and BS ISO 13605:2018 [63], respectively. The trace metals in biomass were evaluated using the ICP-MS based on the standard method ISO BS EN 16968:2015 [64]. Major elements in each biomass were quantified by wavelength dispersive X-ray fluorescence spectrometry (WD-XRF) of the ash based on the standard method BS ISO 13605:2018 [63].

2.2. Thermal conversion of biomass feedstocks

Hydrothermal conversion, pyrolysis, and torrefaction of WW, RS, and LD was investigated using a lab-scale semi-continuous rig, shown in Fig. 1. A detailed description of the process and the experimental

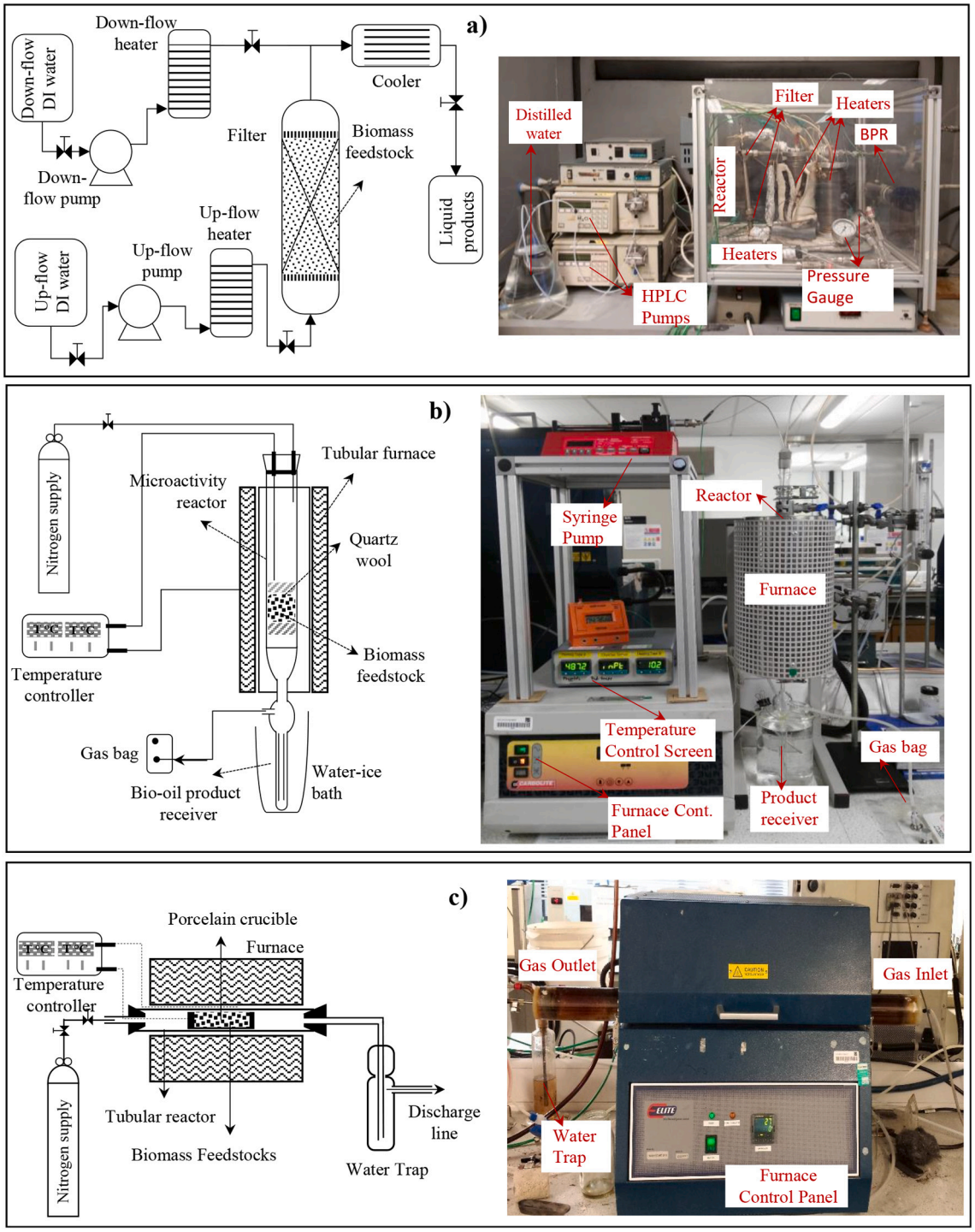

Fig. 1. The process flow diagrams of a) the semi-continuous hydrothermal conversion unit [11,27], b) pyrolysis unit [65] and c) torrefaction unit.

conditions were presented previously [11,58].

Hydrothermal conversion of WW, RS, and LD was investigated at 100 °C (60–2600 psi) for low-temperature extraction, 200 °C (800–3500 psi) for hydrothermal carbonisation, and 300 °C (2000–3500 psi) for hydrothermal liquefaction for ~1.5 h. Approximately 5.0 g of each biomass feedstock was placed between two layers of sieve mesh (100 μm) in the 316 L stainless steel reactor. The hydrothermal rig was pressurised using a downflow of 20 ml/min of distilled water. The heat exchanger temperatures for up flow were then set to the target temperature. Once the system had established at the desired conditions, the up flow was then introduced to the reactor with a flow rate of 20 ml/min. The liquid product stream was cooled to about 20–30 °C in a water-cooled heat exchanger, which was collected and then stored in a freezer at −18 °C for further analysis. The hydrochars were collected from the reactor and dried in an oven at 100 °C for overnight. The chars produced by hydrothermal conversion was defined as "hydrochar" through the manuscript. The pyrolysis tests were investigated in a microactivity test unit [66,67] using the following procedure; approximately 5.0 g of biomass feedstocks (RS, WW, LD) were placed in a micro-activity reactor between two pieces of quartz wool. The reactor was located in the tubular furnace, which was pre-heated to 200 °C. The pyrolysis temperature was then increased to 300,

400 and 550 °C (± 5 °C) with a heating rate of 20 °C/min and kept at this temperature for 60 min under a N_2 flow of 10 ml/min. The bio-oil products were condensed in the liquid product receiver using a water-ice bath, and the gas samples were collected in a 1.0 L gas sampling bag. Experimental error was calculated using a series of experiments carried out in triplicate. The biochars were collected after each experiment and stored in a dry environment. Torrefaction of WW, RS, and LD was also investigated in a horizontal tube furnace system using following procedure; approximately 4.0 g of biomass feedstocks (WW, RS, LD) were placed in a porcelain crucible. The crucible was then placed in the middle zone of a quartz reactor, heated from ambient temperature to the torrefaction temperatures of 220, 250 and 280 °C with a heating rate of 10 °C/min under a N_2 flow rate of 1.0 L/min and the temperature was maintained at this level for 60 min. The porcelain crucible was then removed and cooled to room temperature. The experimental error was determined based on the triplicate of one set of the experiments and results were presented with error bars representing one standard deviation. The chars produced by pyrolysis and torrefaction was defined as "biochar" through this manuscript. Char yield (C_y) of hydrothermal conversion, pyrolysis, and torrefaction was determined using (Eq. (4)) [68]. In order to optimise the char formation and potential applicability of those chars in bioenergy production, energy densification (E_D), energy yield (E_Y), and carbon recovery (C_R, dry ash-free) were determined using the following equations (Eqs. (5) to (7)) [6].

$$C_y\,(wt.\%) = \frac{m_{Char,dry}}{m_{Biomass,dry}} * 100 \tag{4}$$

$$E_D = \frac{HHV_{Char}}{HHV_{Biomass}} \tag{5}$$

$$E_Y\,(wt.\%) = C_y * \frac{HHV_{Char}}{HHV_{Biomass}} \tag{6}$$

$$C_R\,(wt.\%) = C_y * \frac{C_{Char}}{C_{Biomass}} \tag{7}$$

where, $m_{Biomass,\ dry}$ is the dried weight of biomass (g) before thermal conversion, $m_{Char,\ dry}$ is the dried weight of char (g) after thermal conversion of hydrothermal treatment, pyrolysis, and torrefaction. HHV_{Biomas} and HHV_{Char} represent the HHV (kJ/g) of biomass feedstocks and chars. C_{Biomas} and C_{Char} represent the carbon content (dry ash-free) of biomass feedstocks and chars.

2.3. Intrinsic reactivity analysis

Thermogravimetric characterisation, a common method of measuring the intrinsic reactivity of biomass and char samples [48], was used according to the following procedure; approximately 15–25 mg of char (or raw biomass) was placed in a platinum pan. Each sample was heated from ambient temperature to 900 °C with a heating rate of 10 °C/min, under an airflow rate of 100 ml/min, to investigate the intrinsic reactivity of char (and biomass). A derivative plot (dW/dt) provided combustion characteristics for each char such as the initial decomposition temperature (T_{in}), ignition temperature (T_{ig}), temperatures at the peaks (T_{max}), burnout temperature (T_{bo}), maximum weight loss rate (DTG_{max}) and average weight loss rates (DTG_{mean}). In order to evaluate the stability of chars produced by hydrothermal conversion, pyrolysis, and torrefaction and the combustion properties, the combustion stability index (Rw) and the comprehensive combustion index (CCI) were determined by Eqs. (8)–(9) [69].

$$Rw = \frac{DTG_{max}}{T_{ig} * T_{max}} * 8.5875 * 10^7 \tag{8}$$

$$CCI = \frac{DTG_{max} * DTG_{mean}}{T_{ig}^2 * T_{bo}} \tag{9}$$

where, Rw and CCI represent the combustion stability index (wt%/min.°C^2) and comprehensive combustion index (wt%^{2}/min^2.°C^3), respectively. T_{ig} is the ignition temperature (°C), T_{max} temperatures at the highest peak (°C), T_{bo} is burnout temperature (°C), DTG_{max} and DTG_{mean} are the maximum weight loss (wt%/min) rate and average weight loss rates (wt%/min), respectively.

3. Results and discussions

3.1. Characterisation of feedstocks

The characteristics of these feedstocks have been presented previously [11,58]. However, the ultimate and proximate analyses of the biomass feedstocks and biochars (hydrochars) are presented in Supplementary section Table A2. A relatively wide range of trace and major elements was found in the biomass feedstocks as seen in Table 1. These inorganics can catalyse the thermal conversion process [70,71] and combustion [40,66,72], while others increase the fouling tendencies during combustion, decreasing combustion efficiency due to the high heat transfer resistance [73]. WW and LD contain relatively high amounts of Mn (~60 mg/kg) and As (~90 mg/kg), respectively. RS and LD also contain relatively high Mn content, ~24 and ~ 13 mg/kg, respectively and ~ 27–30 mg/kg of Zn. Additionally, the alkali and alkaline metals (i.e., K, Na, S, Cl) impacts on ash chemistry and cause slagging (due to the reactions of alkali metals with silica and produce alkali silicates) and fouling (due to the reactions of alkali metals with sulphur and produce alkali sulphates) [73]. Alkali silicates usually soften and melt at the temperature ~ 700 °C and alkali sulphates can deposited on the surface of reactor where the heat transfer significantly decrease.

3.2. Thermal conversion of biomass feedstocks

Char yields from the thermal conversion of RS, WW and LD through hydrothermal conversion (liquefaction (HTL), carbonisation (HTC) and hydrolysis (HTH)), pyrolysis, and torrefaction are presented in Fig. 2. The increase in the operating temperature of thermal conversion technologies decreases the char yield regardless of the technology. This is in agreement with previous findings [74,75]. The decrease in char yield can be attributed to the gradual thermal decomposition of biomass structure as lignocellulosic biomass begins to carbonise at temperatures above 180 °C [76–78] when the cellulosic and hemicellulosic polymers disintegrate into monomers/oligomers [79]. The main biomass components, hemicellulose, cellulose and lignin, gradually decompose with the temperatures at 220–315 °C, 315–400 °C and at 160–900 °C, respectively [16,56,80]. The extent of decomposition is significantly affected by process conditions. In hydrothermal conversion technologies (Fig. 2a), the temperature has a significant effect on char yield while pressure appears to have a minimal impact on biomass solubility. Each type of biomass contains a different proportion of water-soluble compounds. WW and RS have less water-soluble content (~5–7 wt% and ~ 20 wt%, respectively) compared to LD (~60–65 wt%) at the hydrolysis conditions (HTH, 100–150 °C). When the temperature increases to 200 °C for the hydrothermal carbonisation (HTC, 200 °C), both RS and WW demonstrate similar carbonisation levels with hydrochar yields of ~50 wt%, while LD provides relatively a low hydrochar yield (~10 wt %). During hydrothermal liquefaction (HTL, 300 °C), all three biomass feedstocks demonstrate about ~5–10 wt% char (or solid residue) yield and a 90 wt%, or higher, liquefaction level. Torrefaction is a thermal pre-treatment method converting raw biomass feedstocks into upgraded solid biofuels (biochars) having greater energy density, and calorific value compared to the original biomass feedstock [25,26]. Torrefaction

Table 1
Trace and major element contents of biomass feedstocks analysed by ICP-MS and WD-XRF.

Trace element		Unit	WW	RS	LD	Trace element		Unit	WW	RS	LD
Manganese	**Mn**	mg/kg	60.19	23.6	13.41	**Lead**	**Pb**	mg/kg	0.26	0.37	0.55
Copper	**Cu**	mg/kg	1.37	21.44	2.41	**Tin**	**Sn**	mg/kg	0.66	0.18	0.12
Zinc	**Zn**	mg/kg	4.34	29.61	27.49	**Cadmium**	**Cd**	mg/kg	0.13	0.08	0.12
Nickel	**Ni**	mg/kg	0.89	0.91	2.87	**Antimony**	**Sb**	mg/kg	0.10	0.11	0.10
Chromium	**Cr**	mg/kg	0.38	0.40	3.56	**Cobalt**	**Co**	mg/kg	0.16	0.15	0.29
Arsenic	**As**	mg/kg	0.20	0.10	89.88	**Thallium**	**Tl**	mg/kg	0.10	0.10	0.10
Vanadium	**V**	mg/kg	0.26	0.12	1.41	**Mercury**	**Hg**	mg/kg	0.04	0.04	0.07
Major element		Unit	WW	RS	LD	Major element		Unit	WW	RS	LD
CaO		%	27.06	13.5	5.84	**SiO_2**		%	4.56	0.44	4.26
K_2O		%	18.56	9.84	27.87	**Mn_3O_4**		%	3.18	0.09	0.03
Na_2O		%	1.44	27.99	20	**Al_2O_3**		%	1.08	0.31	0.89
P_2O_5		%	4.98	17.99	1.2	**Fe_2O_3**		%	1.78	0.24	0.37
MgO		%	6.07	6.85	4.95	**TiO_2**		%	0.06	0.02	0.04
SO_3		%	2.98	5.07	9.07						

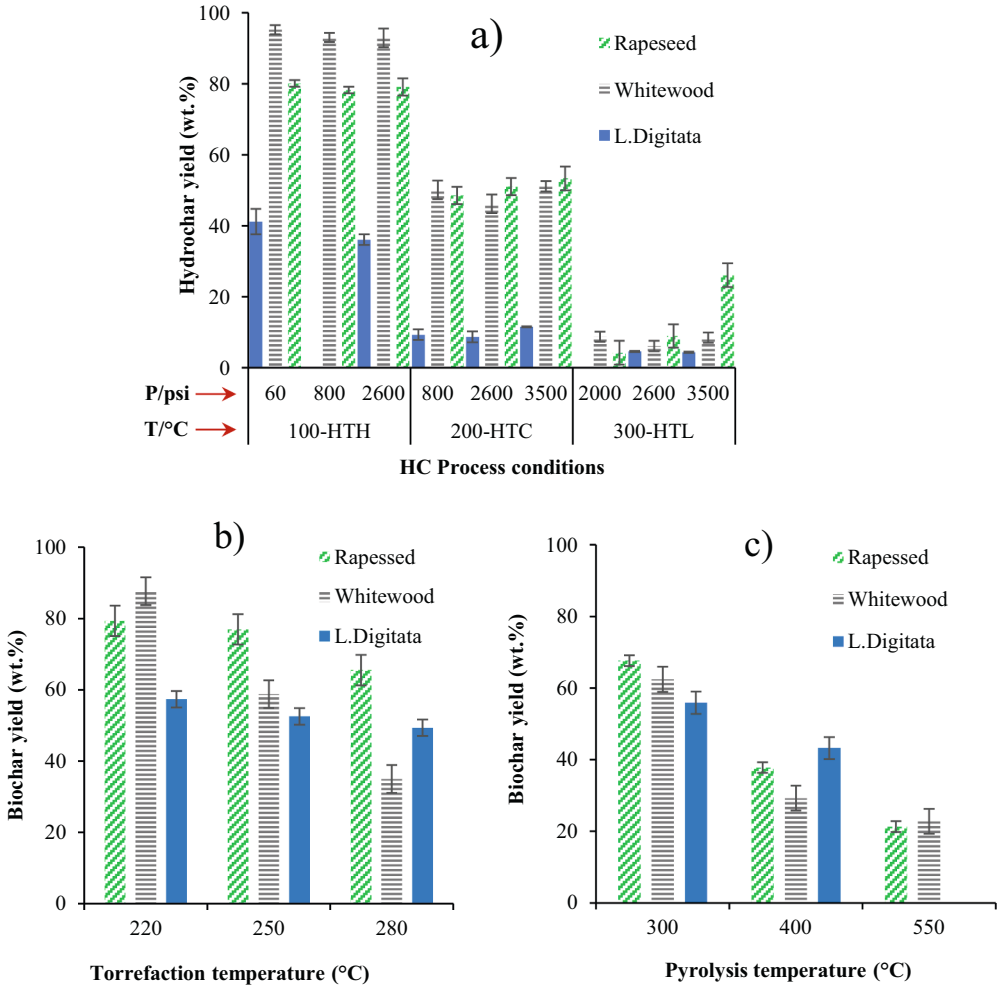

Fig. 2. Char yields of RS, WW, and LD under a) hydrothermal conversion, b) torrefaction and c) pyrolysis. (The abbreviations; HC, PC and TC represents the chars produced by hydrothermal conversion, pyrolysis, and torrefaction, respectively).

is a mild pyrolysis process with temperatures kept at 200–300 °C [81]. WW decomposed most readily via torrefaction to produce a char yield of ~87 wt% at 220 °C droppings significantly to ~35 wt% at 280 °C.

This could be attributed to the hemicellulosic content of WW. Torrefaction of RS and LD did not demonstrate the same level of thermal decomposition. The char yield slightly decreased from 79 to 65 wt% for RS and from 57 to 49 wt% for LD with a temperature increase from 220 to 280 °C (Fig. 2b). During pyrolysis, despite their physicochemical differences, WW and RS behaved similarly and exhibited relatively high thermal decomposition and similar levels of char yield; ~65 wt% at 300 °C, 29–37 wt% at 400 °C and ~ 21 wt% at 550 °C (Fig. 2c). Furthermore, LD also produced relatively high char yields via pyrolysis; 55 wt% at 300 °C and 43 wt% at 400 °C (Fig. 2c) as compared to hydrothermal conversion (Fig. 2a). From Fig. 4a and c, lower char yields

resulted from hydrothermal conversion, compared to pyrolysis, which can be attributed to the different behaviour of water during hydrothermal conversion where it can acts as a solvent, reactant or even a catalyst, depending on the conditions [11].

3.3. Combustion characteristics of the chars (hydrochars/biochars)

The chars produced from WW, RS, and LD by hydrothermal conversion, pyrolysis, and torrefaction were characterised by energy densification, energy yield, and carbon recovery. Furthermore, the change from biomass to char, based on the elemental composition (H/C vs O/C) is plotted using a Van Krevelen diagram. The changes and direction of the position (from biomass to char products) in the Van Krevelen diagram by different biomass processing conditions result from the reactions of dehydration, demethylation, or decarboxylation [46,82,83]. The data for each process is presented separately in Sections 3.3.1to 3.3.2.

3.3.1. Hydrochars produced by hydrothermal conversion

Fig. 3 illustrates the characteristics of hydrochars produced from WW. An increase in the process temperature led to a decrease in energy yield and carbon recovery, whilst increasing the energy densification. The energy yield and carbon recovery for the hydrochars produced at 200 °C are ~50 wt% and decreasing gradually to ~32 wt% at 235 °C, ~15 wt% at 265 °C, and ~ 10 wt% at 300 °C (Fig. 3a). However, the energy densification increases from ~1.0 to ~1.6 with increasing the temperature from 100 to 265 °C (Fig. 3a). As for the effects of pressure, despite a wider range (800–3500 psi), the char characteristics (particularly energy yield, carbon recovery and energy densification) do not change significantly at the early stages of hydrothermal carbonisation (200 °C), as demonstrated in Fig. 3a.

Fig. 3b shows that pressure is also insignificant at 200 °C (as hydrochars (at 200 °C) provide similar H/C and O/C ratios and are located in the Biomass zone in the Van Krevelen diagram. The increase in the conversion temperature decreases the oxygen content and increase the carbon content (Table A2 in Supplementary Section), which results in a shift from biomass zone to Peat (at 235 °C) and then Lignite (at 265 °C) or Coal (at 300 °C) zone in the Van Krevelen Diagram (Fig. 3b). The path through the evaluation of the H/C and O/C atomic ratios in the chars could be attributed to the dehydration reactions, which is similar to previously observed for the hydrothermal conversion of cellulose [82] and saccharides [83].

Fig. 4 shows the characteristics of the hydrochars produced by RS from hydrolysis to liquefaction conditions of the hydrothermal conversion. Hydrochars produced by RS are similar to WW hydrochars, with energy yield and carbon recovery decreasing with an increase in the hydrothermal conversion temperature but with an increase in energy densification (Fig. 4a). The energy yield and carbon recovery of hydrochars produced at 100 °C are ~83 wt% and 80 wt%, respectively. At the same conditions, the hydrochar provides an energy densification of 1.0, which means the HHV of hydrochars is about the same as the raw RS. The energy yield and carbon recovery of hydrochars gradually decrease from ~60 wt% at 200 °C to ~37 wt% at 265 °C, whilst the energy densification increases from 1.1 to 1.4. However, the energy densification of the hydrochars produced at 300 °C decreased to 1.2 due to the liquefaction of RS and increase in ash content. Fig. 4b shows that the hydrochars produced at the hydrolysis (100 °C) and carbonisation (200–265 °C) were shifted to a lower O/C zone which could be attributed to the increase in carbon and decrease in oxygen content (Table A3 in Appendix A), potentially following the decarboxylation path. However, these hydrocars do not show a significant decrease in the H/C ratio as hydrogen content increases with increasing temperature. Conversely, the hydrochar produced at the liquefaction condition (300 °C) provides relatively lower hydrogen contents (Table A3 in Appendix A) as a consequence of demethanation, which enable hydrocar near the Lignite zone in the Van Krevelen diagram.

Among these three biomass feedstocks, LD shows relatively different characteristics as demonstrated in Fig. 5. As previously demonstrated (Fig. 2a), LD demonstrated a significant dissolution at low hydrothermal conversion conditions (below 200 °C), which results in hydrochars having relatively low energy yield and carbon recovery (~13 wt% at 200 °C, Fig. 5a) compared to other biomass feedstocks such as WW (~50 wt% at 200 °C, Fig. 3a) and RS (~57 wt% at 200 °C, Fig. 4a). The energy densification increases from 1.3 to 1.6 by increasing conversion temperatures from 100 °C to 200 °C. Densification then drops to 0.5 at 300 °C, where the char yield is relatively low (5 wt%, Fig. 2a) and ash content is significantly high ~66 wt%. Fig. 5b shows that LD has relatively high O/C and H/C ratios. The LD hydrochars demonstrated a lower O/C ratio with the hydrothermal conversion, but the H/C ratio of LD hydrochars did not show a significant change through the hydrothermal conversion.

Based on the Van Krevelen Diagrams, the impact of the hydrothermal conversion on these three biomass feedstocks could be concluded as;

- The hydrothermal process can produce different types of char structures depending on biomass feedstock type.
- Hydrothermal conversion technology gradually enhances the biomass structure of WW to produce hydrochars with a lower O/C

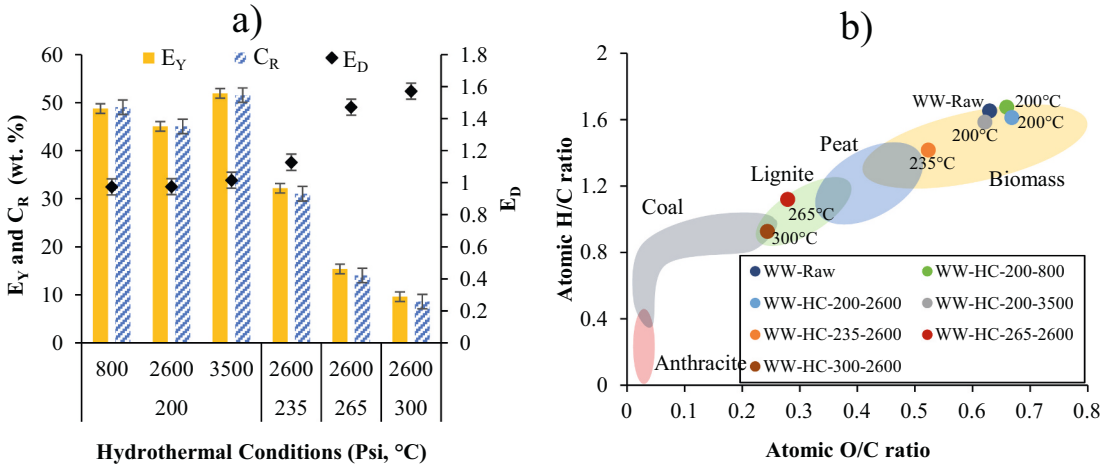

Fig. 3. a) Energy yield (E_Y), Energy densification (E_D), Carbon recovery (C_R), b) Van Krevelen Diagram (atomic ratio of H/C vs O/C) of the hydrochars produced by the hydrothermal conversion of WW.

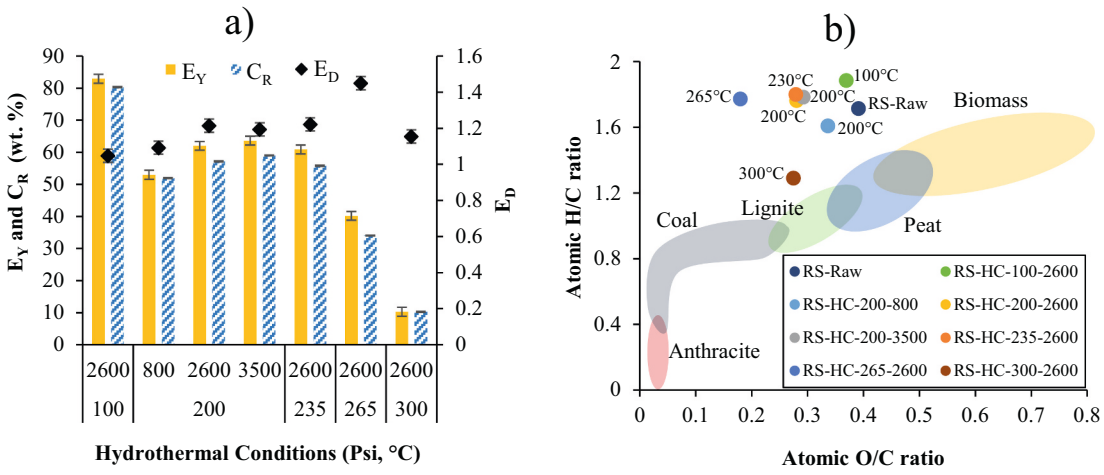

Fig. 4. a) Energy yield (E_Y), Energy densification (E_D), Carbon recovery (C_R), b) Van Krevelen Diagram (atomic ratio of H/C vs O/C) of the hydrochars produced by the hydrothermal conversion of RS.

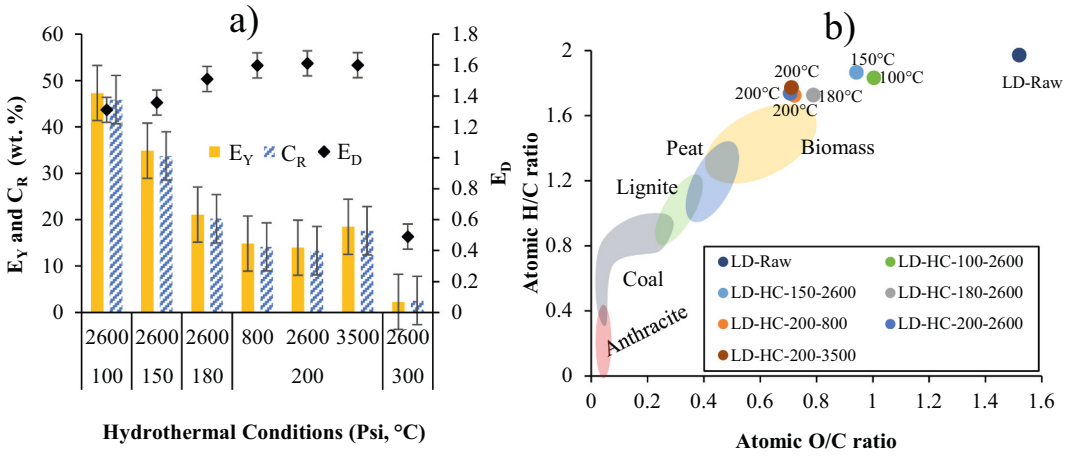

Fig. 5. a) Energy yield (E_Y), Energy densification (E_D), Carbon recovery (C_R), b) Van Krevelen Diagram (atomic ratio of H/C vs O/C) of the hydrochars produced by the hydrothermal conversion of LD.

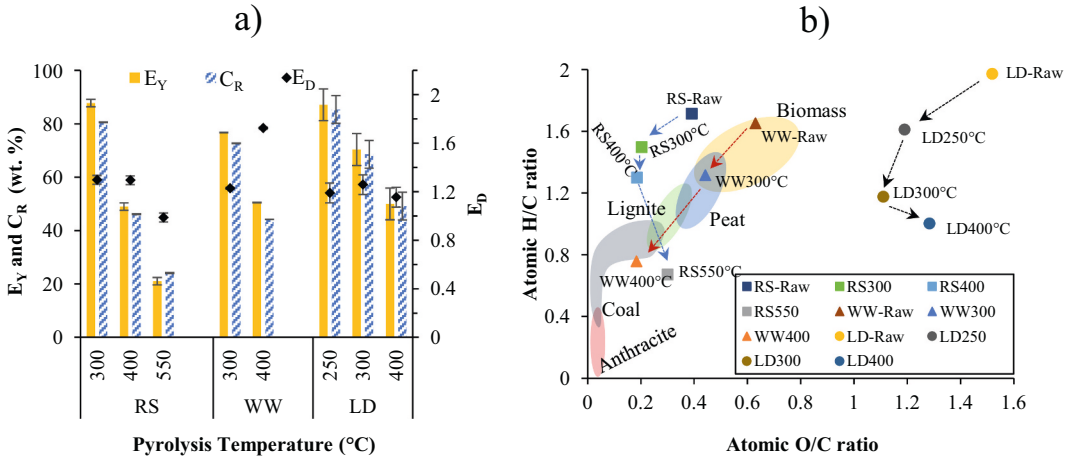

Fig. 6. a) Energy yield (E_Y), Energy densification (E_D), Carbon recovery (C_R), b) Van Krevelen Diagram (atomic ratio of H/C vs O/C) of biochars produced by pyrolysis of RS, WW, and LD.

and H/C ratio, following dehydration reactions. The increase in the temperature enhances the structure from hydrochars to Peat-like and then Lignite-like structures (Fig. 3b).

- The O/C ratio for RS- and LD-based hydrochars decreases with hydrothermal conversion, the H/C ratio did not show a significant change (Figs. 4b and 5b).

3.3.2. Biochars produced by pyrolysis and torrefaction

Fig. 6 shows the combustion characteristics and Van Krevelen Diagram of biochars produced by WW, RS, and LD via pyrolysis. The energy yield of biochars decreased from 88 to 49 wt% for RS, from 77 to 50 wt% for WW, and from 70 to 50 w.% for LD with an increase in temperature from 300 to 400C (Fig. 6a). However, the biochars produced by RS and LD did not show significant energy densification but WW increases significantly from 1.2 to 1.8 for (Fig. 6a). Biochars produced via pyrolysis of WW follows dehydration reactions (Fig. 6b) similar to the hydrochars produced by hydrothermal conversion of WW.

Unlike with hydrothermal conversion, the biochars produced from RS and LD via pyrolysis also showed relatively low O/C-H/C ratios (Fig. 6b), which suggests a dehydration pathway until 400 °C and 300 °C, respectively. Higher pyrolysis temperatures (550 °C for RS and 400 °C for LD) results in methanation. The different reaction paths (dehydration and/or demethanation) could be attributed to the different thermal decomposition mechanisms of biomasses in different processes. As with hydrothermal conversion, the molecular decomposition of biomass feedstocks was driven by the physicochemical properties of the process water, whilst pyrolysis was driven by bond cleavage (bond fission) possible at high temperatures. As shown in Tables A2 and A3, the hydrogen content of hydrochars is not significantly changed after hydrothermal conversion, whilst it gradually decreases with increasing the pyrolysis temperature, which could be attributed to the hydrogen content of water in the hydrothermal conversion.

Fig. 7 shows the combustion characteristics and Van Krevelen Diagram of biochars produced by WW, RS, and LD via torrefaction. The energy yield and carbon recovery decreased from ~93 wt% to ~87 wt% for RS, from ~72 wt% to ~61 wt% for LD, and ~ 89 wt% to ~56 wt% for WW as torrefaction temperature increased from 220 °C to 280 °C (Fig. 7a). The increase in the torrefaction temperature enhances the energy densification (from ~1.0 to ~1.6) for WW-based biochars. However, the enhancement in RS- and LD-based biochars is not as much as that with WW-based biochars. As torrefaction temperatures increased from 220 to 280 °C, the H/C and O/C ratios of WW rapidly decreased (Fig. 7b).

The WW biomass migrates largely along the dehydration line to the state point of WW220, WW250 and WW280 (Fig. 7b), but does not change significantly around the demethylation or decarboxylation line, which is similar to pyrolysis (Fig. 6b) and hydrothermal conversion (Fig. 3b). The H/C and O/C ratios of LD rapidly decrease along the dehydration line to the state point of LD220 with the torrefaction at 220 °C. However, further increase in the torrefaction temperature has an insignificant effect on the ratio of H/C and O/C. Conversely, although the H/C and O/C ratios of RS slowly decrease (Fig. 7b) through the torrefaction temperature along with the dehydration reaction, the differences between RS-Raw and RS280 are therefore insignificant. The dehydration rates of WW and LD are faster than RS.

Based on the Van Krevelen Diagrams, the impact of pyrolysis and torrefaction on these three biomass feedstocks could be concluded as;

- Whilst the biochars produced by pyrolysis and torrefaction usually follow a dehydration type reaction (Figs. 6b and 7b), the impact on the char and change across the Van Krevelen Diagram depends on the biomass type.
- Biochars produced by WW via pyrolysis (Fig. 6b) and torrefaction (Fig. 7b) show the clear migration from higher H/C-O/C levels to much lower H/C-O/C levels through dehydration reaction line. With the increase in the process temperature, the biochars provide peat, lignite, and coal-like structures.
- Pyrolysis gradually enhances the biomass structure of RS and LD through dehydration and then methanation reactions (Fig. 6b), to produce biochars with a lower H/C-O/C ratio. Torrefaction, conversely, did not show the same enhancement of the biochar with increasing temperature (Fig. 7b).

3.4. Intrinsic reactivity of chars

3.4.1. Hydrochars produced by hydrothermal conversion

Fig. 8 shows the thermal degradation characteristics of hydrochars from WW produced at different temperatures through hydrothermal conversion. The characteristic temperatures and intrinsic properties of WW hydrochars are presented in Table 2. Fig. 8a shows weight loss as a function of temperature (and time) while Fig. 8b and c show the rate of weight change as a function of temperature (or time). The raw WW sample exhibits three typical weight loss regions. The first, associated with the combustion of volatile species (peak decomposition rate at 328 °C) [69]. The latter two (observed between 350 and 450 °C, and 450 to 550 °C with a broad peak decomposition rate at 474 °C) are associated with char combustion [69,84] (mainly from lignin and cellulose structures) [11]. The temperature of initial weight loss and the onset of ignition for the raw WW sample were measured as 236 °C and 265 °C (Fig. 8a and Table 2). These have shifted to a higher temperature for the

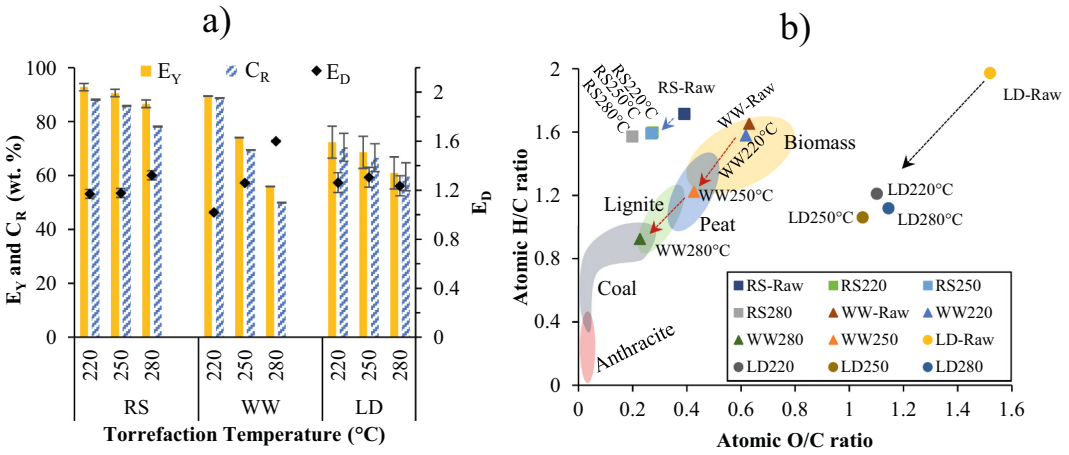

Fig. 7. a) Energy yield (E_Y), Energy densification (E_D), Carbon recovery (C_R), b) Van Krevelen Diagram (atomic ratio of H/C vs O/C) of biochars produced by torrefaction of RS, WW, LD.

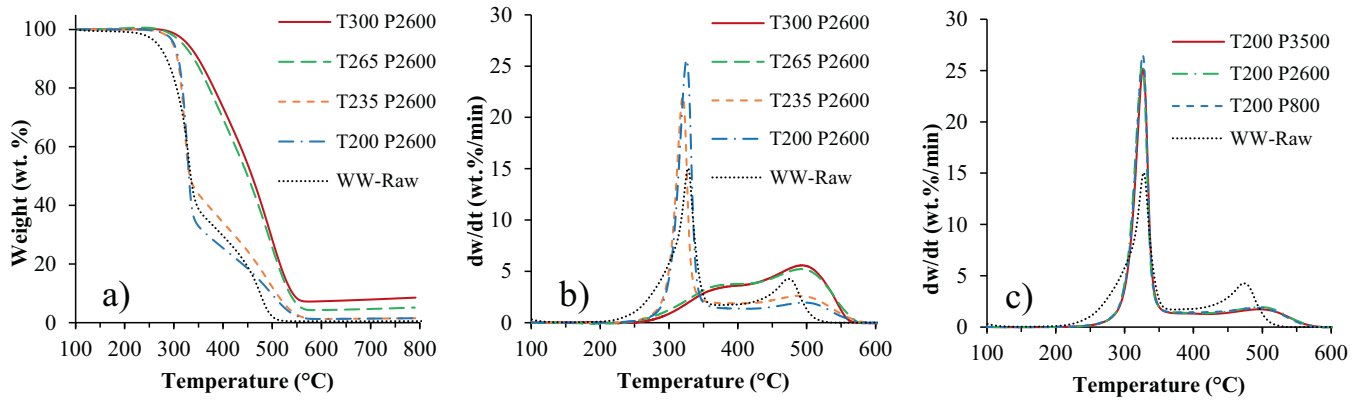

Fig. 8. Intrinsic reactivity results of hydrochars produced by the hydrothermal treatment of WW as weight loss (wt%) and weight-loss rates (wt%/min) of at different temperatures (labelled as "T" in °C) and pressures (labelled as "P" in psi).

Table 2
Characteristic temperatures and intrinsic properties of WW hydrochars.

Hydrochars	T_{in} (°C)	T_{ig} (°C)	T_{max} (°C)	T_{bo} (°C)	DTG_{max} (wt%/min)	DTG_{mean} (wt%/min)	CCI*10^7 (wt%^{2}/min^2°C^3)	Rw*10^5 (wt%/min°C^2)
WW-Raw	236	266	329	509	14.11	3.32	13.01	16.12
WW-HC-T200-P2600	273	289	328	555	25.21	3.42	18.60	26.60
WW-HC-T235-P2600	270	291	322	563	21.83	3.4	15.57	23.30
WW-HC-T265-P2600	274	292	492	566	5.19	3.32	3.57	3.61
WW-HC-T300-P2600	289	313	494	559	5.15	3.24	3.05	3.33
WW-HC-T200-P3500	273	291	328	554	24.87	3.24	17.18	26.06
WW-HC-T200-P2600	273	289	328	555	25.21	3.42	18.60	26.60
WW-HC-T200-P800	273	291	329	553	26.17	3.42	19.11	27.33

Temperatures of initial decomposition (T_{in}), ignition (T_{ig}), peak (T_{max}), and burnout (T_{bo}). Maximum weight loss rate (DTG_{max}) and average weight loss rates (DTG_{mean}) between T_{in}-T_{bo}.

hydrochars produced by hydrothermal conversion (Fig. 8a and Table 2). For the two chars produced at lower temperatures (200 and 235 °C), it is also noticeable that the two latter weight loss regions associated with the combustion of lignin and cellulose have now merged into one, probably through the decomposition of some of the lignin during char formation. Of particular interest is the distinction between the hydrochars produced at temperatures of 235 °C and below versus those produced at 265 °C and above. For the >265 °C hydrochars, the peak temperatures have not only shifted to a higher temperature, but the three main peaks have essentially merged into one distinct peak. This indicates a more severe degradation/loss of the feedstock's hemicellulose and lignin structures and resulting in a more uniform hydrochar structure. This change is evident in the almost complete loss of the first peak in Fig. 8b. These structural changes also resulted in a lower combustion stability index (Rw, ~3.6–3.3*10^{-5}) and a comprehensive combustion index (CCI, ~3.5–3.0*10^{-7}%^{2}/min^2 °C^3). Fig. 8c shows three hydrochar samples produced at the same temperature (200 °C) but with increasing pressures from 800 to 3500 psi. Little observable difference could be seen in terms of the influence of increasing pressure on intrinsic reactivity.

The intrinsic reactivity and characteristic temperatures of hydrochars produced by the hydrothermal conversion of RS are presented in Fig. 9 and Table 3. Several weight loss regions are noticeable for the raw sample in addition to the two to three peak profiles commonly seen for hemicellulosic feedstocks. The additional weight loss peaks and regions are likely due to the degradation of oils present in RS [85].

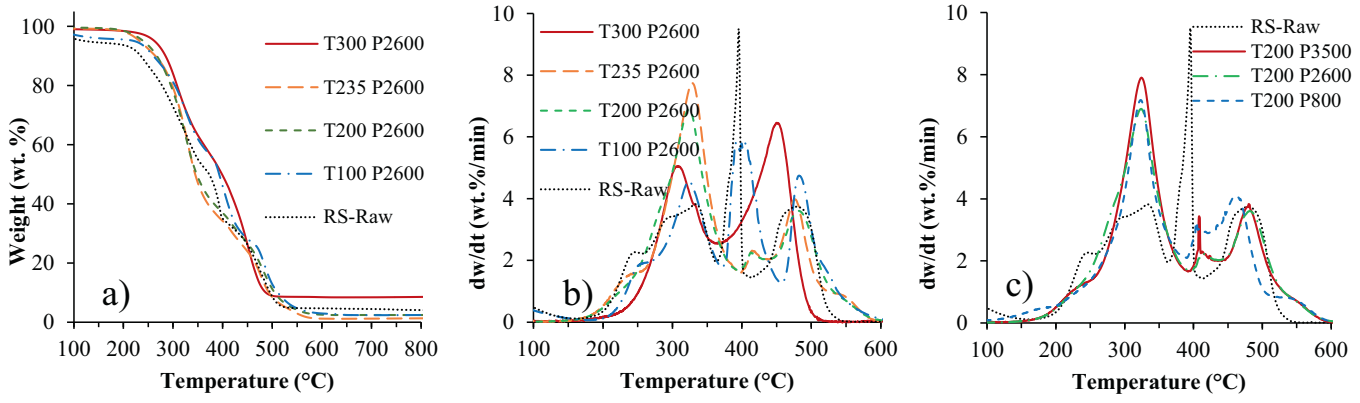

Fig. 9. Intrinsic reactivity results of hydrochars produced by the hydrothermal treatment of RS as weight loss (wt%) and weight-loss rates (wt%/min) of at different temperatures (labelled as "T" in °C) and pressures (labelled as "P" in psi).

Table 3
Characteristic temperatures and intrinsic properties of RS hydrochars.

Hydrochars	T_{in} (°C)	T_{ig} (°C)	T_{max} (°C)	T_{bo} (°C)	DTG_{max} (wt%/min)	DTG_{mean} (wt%/min)	CCI*10^7 (wt%^{2}/min^2°C^3)	Rw*10^5 (wt%/min°C^2)
RS-Raw	197	216	385	513	9.66	2.81	11.34	11.62
RS-HC-T100-P2600	223	233	400	561	5.82	2.69	5.14	6.24
RS-HC-T200-P2600	204	235	324	563	6.89	2.65	5.87	9.05
RS-HC-T235-P2600	197	220	327	564	7.74	2.63	7.46	10.76
RS-HC-T300-P2600	238	263	453	499	6.43	3.39	6.32	5.40
RS-HC-T200-P3500	201	220	327	563	7.89	2.63	7.62	10.97
RS-HC-T200-P2600	204	235	324	563	6.89	2.65	5.87	9.05
RS-HC-T200-P800	188	228	324	567	7.18	2.17	5.29	9.72

Temperatures of initial decomposition (T_{in}), ignition (T_{ig}), peak (T_{max}), and burnout (T_{bo}). Maximum weight loss rate (DTG_{max}) and average weight loss rates (DTG_{mean}) between T_{in}-T_{bo}.

The peak temperatures for the Raw RS and hydrochar produced at 100 °C are 386 °C and 400 °C (Fig. 9b and Table 3), respectively. These temperatures are much lower for the hydrochars produced at HTC conditions (200 °C and 235 °C), which are about ~320–330 °C. However, the peak temperature of hydrochar produced at the HTL conditions (300 °C) was 453 °C, indicating a good relationship between reactivity and proximate analysis (Table A3). Unlike the two higher temperature profiles for WW, for the RS hydrochars, there was a much smaller distinction between the milder versus higher treatment temperatures. Even at 300 °C, RS hydrochar degradation produces a relatively similar profile. Similar to WW chars, the RS hydrochars produced at HTC under different pressure conditions did not show a significant difference in intrinsic reactivity (Fig. 9c) or characteristic temperatures (Table 3). A higher burnout temperature (T_{bo} = ~561–564 °C) was observed for the hydrochars produced at low-temperature hydrothermal conversions (100–235 °C), while slightly lower burnout temperature (499 °C) was observed at the HTL (300 °C) conditions. The structural changes of hydrochars produced at above 265 °C also resulted in a slight decrease in the combustion stability index (Rw, ~3.6–3.3*10^{-5}) and the comprehensive combustion index (CCI, ~3.5–3.0*10^{-7}).

Fig. 10 and Table 4 refer to the oxidative thermal degradation of LD and its hydrochars. The raw LD sample exhibits the 3 main decomposition regions expected for seaweed. At ca. 250 °C, a sharp peak is observable and belongs to the decomposition of alginic acid [86] with the degradation of sugars between 250 and 330 °C and finally the carbon combusting between 400 and 500 °C. As with the changes observed with WW and RS, Fig. 10 also shows a shifting of all main peaks to higher temperatures proportional to hydrochar preparation temperature. At the more extreme temperature of 300 °C, most of the peaks disappear leaving a broad sugar and fixed carbon combustion peak at ~380 °C. As with WW, a distinction can be observed between the hydrochars produced at 300 °C versus lower temperatures indicating that this sample only has fixed carbon left after the hydrotreatment. An increase in pressure did not result in a visible change in the intrinsic reactivity of the samples.

3.4.2. *Biochars produced by pyrolysis and torrefaction*

Intrinsic reactivity results of chars produced by pyrolysis and torrefaction (mild pyrolysis) are presented in Figs. 11 and 12 and Tables 5 and 6. As with the hydrochars, biochars produced by pyrolysis exhibited similar changes as a function of increasing temperature. The main peaks shifted to higher temperatures, and the initial decomposition peaks of lower molecular weight or volatile species disappeared leaving wider peaks associated with fixed carbon combustion (Figs. 11 and 12).

Little distinction can be made between the intrinsic reactivities of hydrochars or those produced from pyrolysis. The combustion stability and the comprehensive combustion indices were very similar for both methods of thermal treatment and varied primarily with temperature, regardless of the technology employed to produce them. WW Biochars appear to be more reactive than those from RS and LD, as is the case with the raw feedstocks.

4. Conclusions

This is novel research that reports an extensive comparative study on the biomass processing pathways (hydrothermal conversion, pyrolysis, and torrefaction) for three distinct biomass feedstocks. The impact of the process is influenced by feedstock type (WW, RS, and LD) in terms of the optimisation of char formation and their combustion characteristics for bioenergy applications. WW char (hydrochar/biochar) was gradually enhanced by hydrothermal conversion, pyrolysis and torrefaction. With the increase in the process temperature, the biochars and hydrochars show lower O/C and H/C ratios, with peat, lignite, and coal-like values. For example, the ratios of (H/C)/(O/C) decreased from ~1.6/0.6 to

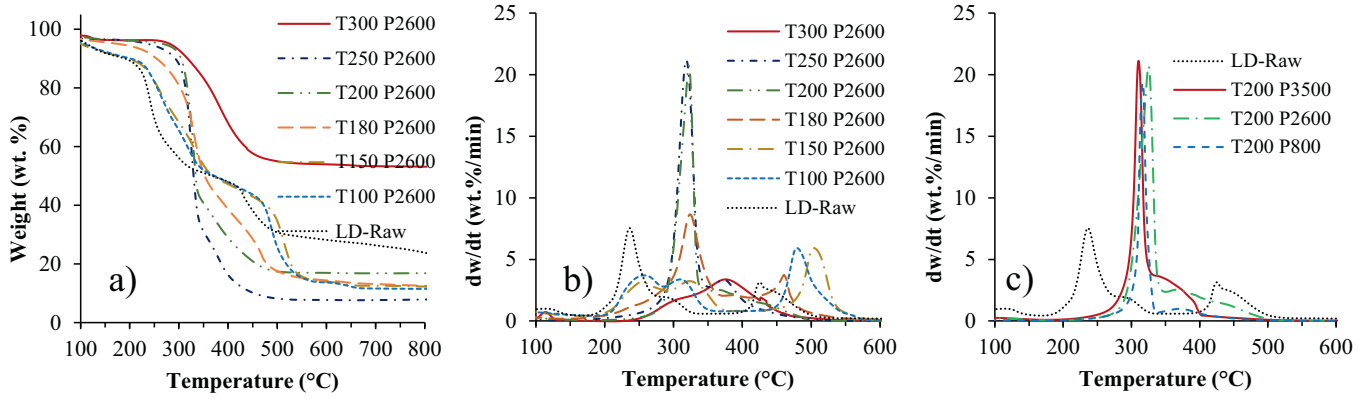

Fig. 10. Intrinsic reactivity results of hydrochars produced by the hydrothermal treatment of LD as weight loss (wt%) and weight-loss rates (wt%/min) of at different temperatures (labelled as "T" in °C) and pressures (labelled as "P" in psi).

Table 4
Characteristic temperatures and intrinsic properties of LD hydrochars.

Hydrochars	T_{in} (°C)	T_{ig} (°C)	T_{max} (°C)	T_{bo} (°C)	DTG_{max} (wt%/min)	DTG_{mean} (wt%/min)	CCI*10^7 (wt%^{2}/min^2°C^3)	Rw*10^5 (wt%/min°C^2)
LD-Raw	184	221	238	503	6.90	1.88	5.28	13.12
LD-HC-T100-P2600	208	234	485	565	5.97	2.11	4.07	5.26
LD-HC-T150-P2600	194	231	510	564	5.94	2.03	4.01	5.04
LD-HC-T180-P2600	212	257	332	518	8.80	2.53	6.51	10.31
LD-HC-T200-P2600	274	304	333	484	22.00	3.65	17.95	21.73
LD-HC-T250-P2600	247	303	327	461	21.76	3.97	20.41	21.96
LD-HC-T300-P2600	268	286	380	469	3.38	1.82	1.60	3.11
LD-HC-T200-P2600	247	293	316	417	33.00	4.42	40.74	35.64
LD-HC-T200-P2600	274	304	333	484	22.00	3.65	17.95	21.73
LD-HC-T200-P2600	252	297	322	446	55.00	3.67	51.31	57.51

Temperatures of initial decomposition (T_{in}), ignition (T_{ig}), peak (T_{max}), and burnout (T_{bo}). Maximum weight loss rate (DTG_{max}) and average weight loss rates (DTG_{mean}) between T_{in}-T_{bo}.

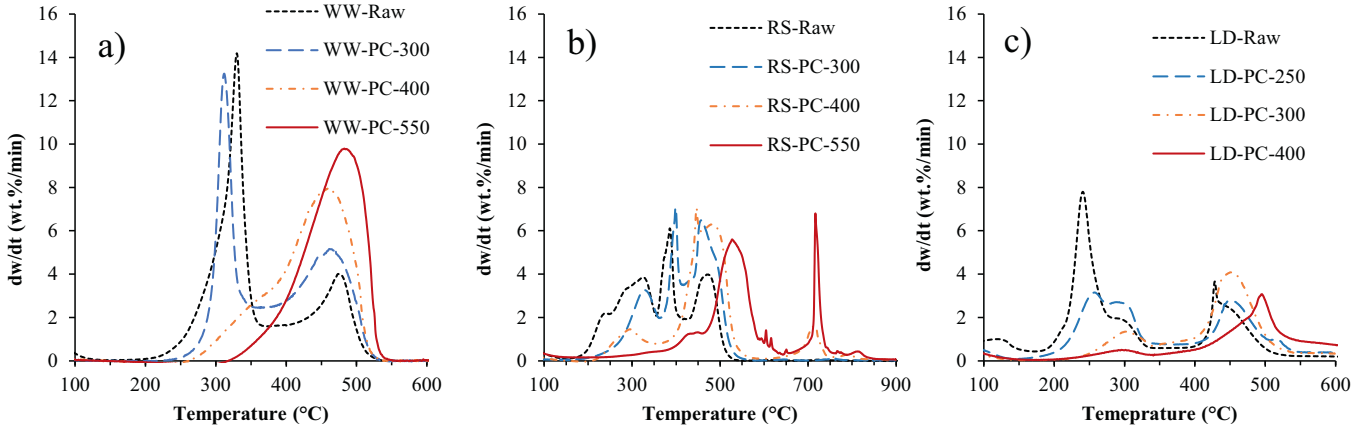

Fig. 11. The weight-loss rates (wt%/min) of intrinsic reactivity of pyrolysis chars of a) WW, b) RS, and c) LD.

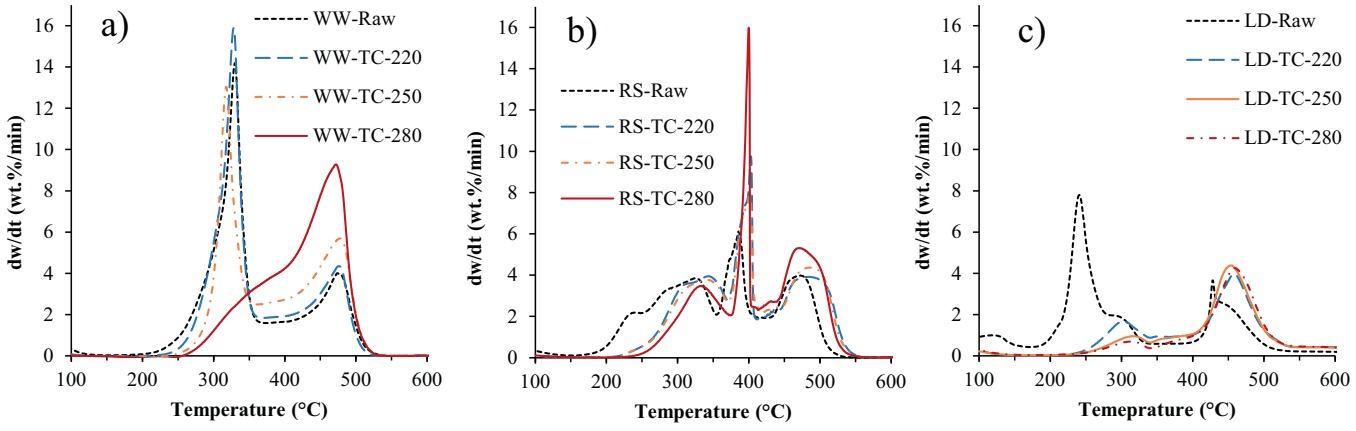

Fig. 12. The weight-loss rates (wt%/min) of intrinsic reactivity of torrefaction chars of a) WW, b) RS, and c) LD.

~0.9/0.2 (lignite/coal like structure) in hydrothermal conversion at 300 °C, to ~0.8/0.2 (lignite/coal like) in torrefaction at 280 °C, and to ~0.7/0.2 (coal like) in pyrolysis at 400 °C. Similarly, the ratio of H/C of RS and LD were gradually enhanced by pyrolysis (decreased from 1.7 to 0.6 for RS and from 1.9 to 1.0 for LD biochars), while the ratio of O/C was insignificantly change by the pyrolysis. Furthermore, the hydrothermal conversion and torrefaction processes had also an insignificant impact on the chars (hydrochar/biochar) structures, where the ratios of (H/C)/(O/C) decreased from 1.7/0.4 to 1.3/0.3 for RS and from 1.9/1.6 to 1.7/0.9 for LD in hydrothermal conversion. As for the intrinsic reactivity, the temperature of initial weight loss and the onset of ignition for the raw biomass sample was shifted to a higher temperature for the hydrochars produced by hydrothermal conversion, i.e. from ~260 °C to ~290–300 °C for WW, from ~216 °C to ~220–260 °C for RS, and from ~221 °C to ~280–300 °C for LD. The peak temperatures of hydrochars produced by WW not only shifted to a higher temperature, but the three main peaks all merged into one distinct peak (at ~490 °C). This convergence indicates a more severe degradation/loss of the feedstock's hemicellulose and lignin structures resulting in a more uniform hydrochar structure at hydrothermal temperatures above 265 °C. Conversely,

Table 5
Characteristic temperatures and intrinsic properties of pyrolysis chars of RS, WW, and LD.

Pyrolysis chars	T_{in} (°C)	T_{ig} (°C)	T_{max} (°C)	T_{bo} (°C)	DTG_{max} (wt%/min)	DTG_{mean} (wt%/min)	$CCI*10^7$ (wt%^{2}/min^2°C^3)	$Rw*10^5$ (wt%/min°C^2)
RS-Raw	197	216	385	513	9.66	2.81	11.34	11.62
WW-Raw	236	266	329	509	14.11	3.32	13.01	16.12
WW-PC-300	253	284	313	518	13.25	3.66	11.61	14.91
WW-PC-400	274	305	457	519	7.92	3.92	6.43	5.68
WW-PC-550	330	371	483	531	9.77	4.9	6.55	5.45
RS-Raw	197	216	385	513	9.66	2.81	11.34	11.62
RS-PC-300	213	278	399	527	6.99	2.86	4.91	6.30
RS-PC-400	229	251	446	733	7.06	1.68	2.57	6.31
RS-PC-550	263	391	716	746	6.788	1.52	0.90	2.42
LD-Raw	184	221	238	503	6.90	1.88	5.28	13.12
LD-PC-250	181	227	257	537	3.15	1.49	1.70	5.40
LD-PC-300	237	267	453	523	4.07	1.48	1.62	3.36
LD-PC-400	241	250	495	644	3.02	0.86	0.65	2.44

Temperatures of initial decomposition (T_{in}), ignition (T_{ig}), peak (T_{max}), and burnout (T_{bo}). Maximum weight loss rate (DTG_{max}) and average weight loss rates (DTG_{mean}) between T_{in}-T_{bo}.

Table 6
Characteristic temperatures and intrinsic properties of torrefaction chars of RS, WW, and LD.

Torrefaction chars	T_{in} (°C)	T_{ig} (°C)	T_{max} (°C)	T_{bo} (°C)	DTG_{max} (wt%/min)	DTG_{mean} (wt%/min)	$CCI*10^7$ (wt%^{2}/min^2°C^3)	$Rw*10^5$ (wt%/min°C^2)
WW-Raw	236	266	329	509	14.11	3.32	13.01	16.12
WW-TC-220	255	285	328	506	15.61	3.75	14.24	16.70
WW-TC-250	269	294	318	515	13.03	3.87	11.33	13.94
WW-TC-280	280	302	473	514	9.269	4.12	8.15	6.49
RS-Raw	197	216	385	513	9.66	2.81	11.34	11.62
RS-TC-220	246	273	403	537	9.56	3.14	7.50	8.69
RS-TC-250	248	267	402	535	8.02	3.14	6.60	7.47
RS-TC-280	264	280	400	529	15.88	3.38	12.94	14.18
LD-Raw	186	223	240	503	7.775	1.88	5.84	14.53
LD-TC-220	243	266	458	530	3.972	1.49	1.58	3.26
LD-TC-250	254	275	454	531	4.376	1.47	1.60	3.51
LD-TC-280	257	273	459	538	4.253	1.35	1.43	3.39

Temperatures of initial decomposition (T_{in}), ignition (T_{ig}), peak (T_{max}), and burnout (T_{bo}). Maximum weight loss rate (DTG_{max}) and average weight loss rates (DTG_{mean}) between T_{in}-T_{bo}.

hydrochars produced by RS showed a much smaller distinction between the milder versus higher treatment temperatures; even at 300 °C, RS hydrochar degradation follows a relatively similar shape. Pressure (with HTC) did not have a significant impact on intrinsic reactivity regardless of biomass feedstocks. This study demonstrates how the optimal holistic biomass processing pathways and process interdependencies are influenced by feedstocks and process conditions. The formation of char and their characteristics directly influence their potential use in bioenergy production.

CRediT authorship contribution statement

Fatih Güleç: Conceptualization, Formal analysis, Investigation, Validation, Visualization, Writing – original draft, Writing – review & editing. **Abby Samson:** Methodology, Funding acquisition, Writing – original draft, Writing – review & editing. **Orla Williams:** Conceptualization, Funding acquisition, Methodology, Supervision, Writing – review & editing. **Emily T. Kostas:** Methodology, Funding acquisition, Writing – review & editing. **Edward Lester:** Conceptualization, Methodology, Supervision, Project administration, Funding acquisition, Writing – review & editing.

Declaration of Competing Interest

The authors declare that they have no known competing financial interests or personal relationships that could have appeared to influence the work reported in this paper.

Data availability

Data will be made available on request.

Acknowledgements

This research was funded and supported by the EPSRC, BBSRC and UK Supergen Bioenergy Hub [Grant number EP/S000771/1], the University of Nottingham Anne McLaren Research Fellowship (Dr Orla Williams), and the UK Biotechnology and Biological Sciences Research Council (BBSRC) Discovery Fellowship (Dr Emily Kostas) [Grant number BB/S010610/1]. We also would like to acknowledge Dr. David Gray, Dr. Filippo Bramante, and Dr. Vincenzo Di Bari for supplying Rapeseed for this project.

Appendix A. Supplementary data

Supplementary data to this article can be found online at https://doi.org/10.1016/j.fuproc.2022.107492.

References

[1] M. Kumar, A.O. Oyedun, A. Kumar, A review on the current status of various hydrothermal technologies on biomass feedstock, Renew. Sust. Energ. Rev. 81 (2018) 1742–1770.
[2] E.T. Kostas, O.S. Williams, G. Duran-Jimenez, A.J. Tapper, M. Cooper, R. Meehan, J.P. Robinson, Microwave pyrolysis of *Laminaria digitata* to produce unique seaweed-derived bio-oils, Biomass Bioenergy 125 (2019) 41–49.
[3] J.A. Okolie, E.I. Epelle, M.E. Tabat, U. Orivri, A.N. Amenaghawon, P.U. Okoye, B. Gunes, Waste biomass valorization for the production of biofuels and value-

added products: a comprehensive review of thermochemical, biological and integrated processes, Process. Saf. Environ. Prot. 159 (2022) 323–344.
[4] S. Jha, J.A. Okolie, S. Nanda, A.K. Dalai, A review of biomass resources and thermochemical conversion technologies, Chem. Eng. Technol. 45 (2022) 791–799.
[5] S.P. Andersen, B. Allen, G.C. Domingo, Biomass in the EU Green Deal: Towards Consensus on the Use of Biomass for EU Bioenergy, Institute for European Environmental Policy (IEEP), 2021.
[6] P.J. Arauzo, M. Atienza-Martínez, J. Ábrego, M.P. Olszewski, Z. Cao, A. Kruse, Combustion characteristics of hydrochar and pyrochar derived from digested sewage sludge, Energies 13 (2020) 4164.
[7] F. Fan, X. Xing, S. Shi, X. Zhang, X. Zhang, Y. Li, Y. Xing, Combustion characteristic and kinetics analysis of hydrochars, Trans. Chin. Soc. Agric. Eng. 32 (2016) 219–224.
[8] F. Xie, B. Zhang, N. Wang, Non-linear relationship between energy consumption transition and green total factor productivity: a perspective on different technology paths, Sustain. Prod. Consum. 28 (2021) 91–104.
[9] N. Scarlat, J. Dallemand, N. Taylor, M. Banja, J. Sanchez Lopez, M. Avraamides, Brief on Biomass for Energy in the European Union, Publications Office of the European Union, Luxembourg, 2019.
[10] E. Comission, Bioeconomy: The European Way to Use Our Natural Resources. Action Plan 2018, Office of the European Union Brussels, Belgium, 2018.
[11] F. Güleç, L.M.G. Riesco, O. Williams, E.T. Kostas, A. Samson, E. Lester, Hydrothermal conversion of different lignocellulosic biomass feedstocks–effect of the process conditions on hydrochar structures, Fuel 302 (2021), 121166.
[12] J. Pfersich, P.J. Arauzo, M. Lucian, P. Modugno, M.-M. Titirici, L. Fiori, A. Kruse, Hydrothermal conversion of spent sugar beets into high-value platform molecules, Molecules 25 (2020) 3914.
[13] K. Alper, K. Tekin, S. Karagöz, A.J. Ragauskas, Sustainable energy and fuels from biomass: a review focusing on hydrothermal biomass processing, Sustain. Energy Fuels 4 (2020) 4390–4414.
[14] E.T. Kostas, G. Durán-Jiménez, B.J. Shepherd, W. Meredith, L.A. Stevens, O. S. Williams, G.J. Lye, J.P. Robinson, Microwave pyrolysis of olive pomace for bio-oil and bio-char production, Chem. Eng. J. 387 (2020), 123404.
[15] S. Wang, G. Dai, H. Yang, Z. Luo, Lignocellulosic biomass pyrolysis mechanism: a state-of-the-art review, Prog. Energy Combust. Sci. 62 (2017) 33–86.
[16] H. Yang, R. Yan, H. Chen, D.H. Lee, C. Zheng, Characteristics of hemicellulose, cellulose and lignin pyrolysis, Fuel 86 (2007) 1781–1788.
[17] N. Abdoulmoumine, S. Adhikari, A. Kulkarni, S. Chattanathan, A review on biomass gasification syngas cleanup, Appl. Energy 155 (2015) 294–307.
[18] L. Cao, K. Iris, X. Xiong, D.C. Tsang, S. Zhang, J.H. Clark, C. Hu, Y.H. Ng, J. Shang, Y.S. Ok, Biorenewable hydrogen production through biomass gasification: a review and future prospects, Environ. Res. 186 (2020), 109547.
[19] F.H. Isikgor, C.R. Becer, Lignocellulosic biomass: a sustainable platform for the production of bio-based chemicals and polymers, Polym. Chem. 6 (2015) 4497–4559.
[20] M. Guo, W. Song, The growing US bioeconomy: drivers, development and constraints, New Biotechnol. 49 (2019) 48–57.
[21] F. Güleç, E.H. Şimşek, H.T. Sarı, Prediction of biomass pyrolysis mechanisms and kinetics–application of Kalman filter, Chem. Eng. Technol. 45 (2022) 167–177.
[22] F. Güleç, G.D.T. Özdemir, Investigation of drying characteristics of Cherry Laurel (*Laurocerasus officinalis* Roemer) fruits, Akademik ziraat dergisi 6 (2017) 73–80.
[23] A.I. Osman, N. Mehta, A.M. Elgarahy, A. Al-Hinai, H. Ala'a, D.W. Rooney, Conversion of biomass to biofuels and life cycle assessment: a review, Environ. Chem. Lett. (2021) 1–44.
[24] D. Pandey, A. Daverey, K. Arunachalam, Biochar: production, properties and emerging role as a support for enzyme immobilization, J. Clean. Prod. 255 (2020), 120267.
[25] D.R. Nhuchhen, P. Basu, B. Acharya, A comprehensive review on biomass torrefaction, Int. J. Renew. Energy Biofuels 2014 (2014) 1–56.
[26] J.G. Pohlmann, E. Osório, A.C. Vilela, M.A. Diez, A.G. Borrego, Integrating physicochemical information to follow the transformations of biomass upon torrefaction and low-temperature carbonization, Fuel 131 (2014) 17–27.
[27] F. Güleç, O. Williams, E.T. Kostas, A. Samson, L.A. Stevens, E. Lester, A comprehensive comparative study on methylene blue removal from aqueous solution using biochars produced from rapeseed, whitewood, and seaweed (*Laminaria Digitata*) via different thermal conversion technologies, Fuel 330 (2022), 125428.
[28] D. Lachos-Perez, P.C. Torres-Mayanga, E.R. Abaide, G.L. Zabot, F. De Castilhos, Hydrothermal carbonization and liquefaction: differences, progress, challenges, and opportunities, Bioresour. Technol. 343 (2022), 126084.
[29] T. Evcil, H. Simsir, S. Ucar, K. Tekin, S. Karagoz, Hydrothermal carbonization of lignocellulosic biomass and effects of combined Lewis and Brønsted acid catalysts, Fuel 279 (2020).
[30] W.-H. Chen, B.-J. Lin, Y.-Y. Lin, Y.-S. Chu, A.T. Ubando, P.L. Show, H.C. Ong, J.-S. Chang, S.-H. Ho, A.B. Culaba, Progress in biomass torrefaction: principles, applications and challenges, Prog. Energy Combust. Sci. 82 (2021), 100887.
[31] T.A. Mamvura, G. Danha, Biomass torrefaction as an emerging technology to aid in energy production, Heliyon 6 (2020), e03531.
[32] J.J. Manyà, Pyrolysis for biochar purposes: a review to establish current knowledge gaps and research needs, Environ. Sci. Technol. 46 (2012) 7939–7954.
[33] L. Zhao, X. Cao, O. Mašek, A. Zimmerman, Heterogeneity of biochar properties as a function of feedstock sources and production temperatures, J. Hazard. Mater. 256 (2013) 1–9.
[34] A. El-Naggar, A.H. El-Naggar, S.M. Shaheen, B. Sarkar, S.X. Chang, D.C. Tsang, J. Rinklebe, Y.S. Ok, Biochar composition-dependent impacts on soil nutrient release, carbon mineralization, and potential environmental risk: a review, J. Environ. Manag. 241 (2019) 458–467.
[35] D. Mohan, K. Abhishek, A. Sarswat, M. Patel, P. Singh, C.U. Pittman, Biochar production and applications in soil fertility and carbon sequestration–a sustainable solution to crop-residue burning in India, RSC Adv. 8 (2018) 508–520.
[36] H. Demir, A. Top, D. Balköse, S. Ülkü, Dye adsorption behavior of *Luffa cylindrica* fibers, J. Hazard. Mater. 153 (2008) 389–394.
[37] F. Ferrero, Dye removal by low cost adsorbents: hazelnut shells in comparison with wood sawdust, J. Hazard. Mater. 142 (2007) 144–152.
[38] G. Annadurai, R.-S. Juang, D.-J. Lee, Use of cellulose-based wastes for adsorption of dyes from aqueous solutions, J. Hazard. Mater. 92 (2002) 263–274.
[39] S. Román, J.M.V. Nabais, C. Laginhas, B. Ledesma, J.F. González, Hydrothermal carbonization as an effective way of densifying the energy content of biomass, Fuel Process. Technol. 103 (2012) 78–83.
[40] F. Güleç, W. Meredith, C.-G. Sun, C.E. Snape, Selective low temperature chemical looping combustion of higher alkanes with Cu-and Mn-oxides, Energy 173 (2019) 658–666.
[41] F. Güleç, D. Pekaslan, O. Williams, E. Lester, Predictability of higher heating value of biomass feedstocks via proximate and ultimate analyses–a comprehensive study of artificial neural network applications, Fuel 320 (2022), 123944.
[42] B. Gunes, A critical review on biofilm-based reactor systems for enhanced syngas fermentation processes, Renew. Sust. Energ. Rev. 143 (2021), 110950.
[43] P.K. Dikshit, H.-B. Jun, B.S. Kim, Biological conversion of lignin and its derivatives to fuels and chemicals, Korean J. Chem. Eng. 37 (2020) 387–401.
[44] L. Chen, C. Wen, W. Wang, T. Liu, E. Liu, H. Liu, Z. Li, Combustion behaviour of biochars thermally pretreated via torrefaction, slow pyrolysis, or hydrothermal carbonisation and co-fired with pulverised coal, Renew. Energy 161 (2020) 867–877.
[45] F. Güleç, A. Erdogan, P.T. Clough, E. Lester, Investigation of the hydrodynamics in the regenerator of fluid catalytic cracking unit integrated by chemical looping combustion, Fuel Process. Technol. 223 (2021), 106998.
[46] Y. Xu, M. Xia, Y. Jiang, F. Li, B. Xue, Opal promotes hydrothermal carbonization of hydroxypropyl methyl cellulose and formation of carbon nanospheres, RSC Adv. 8 (2018) 20095–20107.
[47] Q. Lang, Z. Liu, Y. Li, J. Xu, J. Li, B. Liu, Q. Sun, Combustion characteristics, kinetic and thermodynamic analyses of hydrochars derived from hydrothermal carbonization of cattle manure, J. Environ. Chem. Eng. 10 (2022), 106938.
[48] E. Sima-Ella, G. Yuan, T. Mays, A simple kinetic analysis to determine the intrinsic reactivity of coal chars, Fuel 84 (2005) 1920–1925.
[49] W. Cao, J. Li, L. Lue, Study on the ignition behavior and kinetics of combustion of biomass, Energy Procedia 142 (2017) 136–141.
[50] A.K. Burnham, Van Krevelen diagrams, in: R. Sorkhabi (Ed.), Encyclopedia of Petroleum Geoscience, Springer International Publishing, Cham, 2018, pp. 1–5.
[51] Y. Gao, J. Remón, A.S. Matharu, Microwave-assisted hydrothermal treatments for biomass valorisation: a critical review, Green Chem. 23 (2021) 3502–3525.
[52] O. Williams, G. Newbolt, C. Eastwick, S. Kingman, D. Giddings, S. Lormor, E. Lester, Influence of mill type on densified biomass comminution, Appl. Energy 182 (2016) 219–231.
[53] E.T. Kostas, D.A. White, D.J. Cook, Development of a bio-refinery process for the production of speciality chemical, biofuel and bioactive compounds from *Laminaria digitata*, Algal Res. 28 (2017) 211–219.
[54] S. Paczkowski, C. Sauer, A. Anetzberger, M. Paczkowska, M. Russ, M. Wöhler, S. Pelz, Feedstock particle size distribution and water content dynamic in a pellet mill production process and comparative sieving performance of horizontal 3.15-mm mesh and 3.15-mm hole sieves, Biomass Convers. Biorefin. (2019) 1–12.
[55] EN-ISO-17827-2, Solid Biofuels - Determination of Particle Size Distribution for Uncompressed Fuels: Part 2: Vibrating Screen Method using Sieves with Aperture of 3,15 mm and below (17827-2:2016-10), DIN Deutsches Insitut für Normung, 2016.
[56] E. Lester, M. Gong, A. Thompson, A method for source apportionment in biomass/coal blends using thermogravimetric analysis, J. Anal. Appl. Pyrolysis 80 (2007) 111–117.
[57] J. Adams, A. Ross, K. Anastasakis, E. Hodgson, J. Gallagher, J. Jones, I. Donnison, Seasonal variation in the chemical composition of the bioenergy feedstock *Laminaria digitata* for thermochemical conversion, Bioresour. Technol. 102 (2011) 226–234.
[58] F. Güleç, O. Williams, E.T. Kostas, A. Samson, E. Lester, Optimisation of biochar/hydrochar formation from different biomass feedstocks via hydrothermal conversion, pyrolysis, and torrefaction – A comparative evaluation of biochar/hydrochar structures, The University of Nottingham, 2022.
[59] C.-Y. Yin, Prediction of higher heating values of biomass from proximate and ultimate analyses, Fuel 90 (2011) 1128–1132.
[60] A. Callejón-Ferre, B. Velázquez-Martí, J. López-Martínez, F. Manzano-Agugliaro, Greenhouse crop residues: energy potential and models for the prediction of their higher heating value, Renew. Sust. Energ. Rev. 15 (2011) 948–955.
[61] D.A. Tillman, Wood as an Energy Resource, Elsevier, 2012.
[62] BSI, Solid Biofuels—Determination of Total Content of Carbon, Hydrogen and Nitrogen, BSI Standards Publication, Bonn, Germany, 2015.
[63] BSI, Solid Mineral Fuels — Major and Minor Elements in Coal Ash and Coke Ash — Wavelength Dispersive X-Ray Fluorescence Spectrometric Method, BSI Standards Publication, 2018.
[64] BSI, Solid Biofuels—Determination of Minor Elements; BSI Standards Publication, BSI Standards Publication, Bonn, Germany, 2015.
[65] F. Güleç, Demonstrating the applicability of chemical looping combustion for fluid catalytic cracking unit as a novel CO2 capture technology, in: Chemical Engineering, University of Nottingham, 2020.

[66] F. Güleç, W. Meredith, C.-G. Sun, C.E. Snape, A novel approach to CO2 capture in fluid catalytic cracking—chemical looping combustion, Fuel 244 (2019) 140–150.
[67] F. Güleç, W. Meredith, C.-G. Sun, C.E. Snape, Demonstrating the applicability of chemical looping combustion for the regeneration of fluid catalytic cracking catalysts, Chem. Eng. J. 389 (2020), 124492.
[68] J. Koechermann, K. Goersch, B. Wirth, J. Muehlenberg, M. Klemm, Hydrothermal carbonization: temperature influence on hydrochar and aqueous phase composition during process water recirculation, J. Environ. Chem. Eng. 6 (2018) 5481–5487.
[69] Q. Lang, H. Luo, Y. Li, D. Li, Z. Liu, T. Yang, Thermal behavior of hydrochar from co-hydrothermal carbonization of swine manure and sawdust: effect of process water recirculation, Sustain. Energy Fuels 3 (2019) 2329–2336.
[70] A. Niftaliyeva, F. Güleç, A. Karaduman, Methylation of 2-methylnaphthalene over metal-impregnated mesoporous MCM-41 for the synthesis of 2, 6-triad dimethylnaphthalene isomers, Res. Chem. Intermed. 46 (2020) 2403–2416.
[71] F. Güleç, A. Özen, A. Niftaliyeva, A. Aydın, E.H. Şimşek, A. Karaduman, A kinetic study on methylation of naphthalene over Fe/ZSM-5 zeolite catalysts, Res. Chem. Intermed. 44 (2018) 55–67.
[72] E.H. Şimşek, F. Güleç, F.S. Akçadağ, Understanding the liquefaction mechanism of Beypazarı lignite in tetralin with ultraviolet irradiation using discrete time models, Fuel Process. Technol. 198 (2020), 106227.
[73] A.M. Smith, S. Singh, A.B. Ross, Fate of inorganic material during hydrothermal carbonisation of biomass: influence of feedstock on combustion behaviour of hydrochar, Fuel 169 (2016) 135–145.
[74] S. Chandra, J. Bhattacharya, Influence of temperature and duration of pyrolysis on the property heterogeneity of rice straw biochar and optimization of pyrolysis conditions for its application in soils, J. Clean. Prod. 215 (2019) 1123–1139.
[75] S.-X. Zhao, N. Ta, X.-D. Wang, Effect of temperature on the structural and physicochemical properties of biochar with apple tree branches as feedstock material, Energies 10 (2017) 1293.
[76] D.C. Elliott, P. Biller, A.B. Ross, A.J. Schmidt, S.B. Jones, Hydrothermal liquefaction of biomass: developments from batch to continuous process, Bioresour. Technol. 178 (2015) 147–156.
[77] M. Heidari, A. Dutta, B. Acharya, S. Mahmud, A review of the current knowledge and challenges of hydrothermal carbonization for biomass conversion, J. Energy Inst. 92 (2019) 1779–1799.
[78] O. Arellanoa, M. Flores, J. Guerra, A. Hidalgo, D. Rojas, A. Strubinger, Hydrothermal carbonization (HTC) of corncob and characterization of the obtained hydrochar, Chem. Eng. 50 (2016).
[79] K. Tekin, S. Karagöz, S. Bektaş, A review of hydrothermal biomass processing, Renew. Sust. Energ. Rev. 40 (2014) 673–687.
[80] M. Carrier, L. Auret, A. Bridgwater, J.H. Knoetze, Using apparent activation energy as a reactivity criterion for biomass pyrolysis, Energy Fuel 30 (2016) 7834–7841.
[81] M. Wilk, A. Magdziarz, Hydrothermal carbonization, torrefaction and slow pyrolysis of Miscanthus giganteus, Energy 140 (2017) 1292–1304.
[82] M. Sevilla, A.B. Fuertes, The production of carbon materials by hydrothermal carbonization of cellulose, Carbon 47 (2009) 2281–2289.
[83] M. Sevilla, A.B. Fuertes, Chemical and structural properties of carbonaceous products obtained by hydrothermal carbonization of saccharides, Chem. Eur. J. 15 (2009) 4195–4203.
[84] M. Xu, C. Sheng, Influences of the heat-treatment temperature and inorganic matter on combustion characteristics of cornstalk biochars, Energy Fuel 26 (2012) 209–218.
[85] E.Ü. Çulcuoğlu, Filiz Karaosmanoğlu Esin, Thermogravimetric analysis of the rapeseed cake, Energy Sources 23 (2001) 889–895.
[86] E. Membere, P. Sallis, Thermochemical characterization of brown seaweed, *Laminaria digitata* from UK shores, J. Anal. Appl. Pyrolysis 131 (2018) 42–51.